Rising Thermal

The goal of this investigation was to solve the following two-dimensional Boussinesq equation system:

$$\frac{\partial \omega}{\partial t} = -J(\psi, \omega) - \frac{g}{\theta_0}\frac{\partial \theta}{\partial x} \tag{1}$$

$$\frac{\partial \theta}{\partial t} = -J(\psi, \theta) \tag{2}$$

$$\frac{\partial^2 \psi}{\partial x^2} + \frac{\partial^2 \psi}{\partial z^2} = -\omega \tag{3}$$

The discretization scheme involves three methods of calculating the Jacobian as outlined in the report for Modeling Task 6. The Arakawa discretization then uses the average of the three to advect the solution. Both vertical velocity (ω) and potential temperature (θ) were advanced in time one after the other using Euler-Forward (equations (4) and (5)) for the first two time steps, followed by AB3 (equations (6) and (7)) for the remainder of the 1500 seconds of observation. After this, stream function was calculated by running the successive over relaxation (SOR) scheme to solve the Poisson equation as in Modeling Task 5.

$$\omega_{i,j}^{n+1} = \omega_{i,j}^{n} - \left[J(\psi, \omega)\right]_{i,j}^{n} \cdot \Delta t - \frac{g}{\theta_0}\frac{\theta_{i+1,j}^{n} - \theta_{i-1,j}^{n}}{2\Delta x} \cdot \Delta t \tag{4}$$

$$\theta_{i,j}^{n+1} = \theta_{i,j}^{n} - \left[J(\psi, \theta)\right]_{i,j}^{n} \cdot \Delta t \tag{5}$$

$$\begin{aligned} \omega_{i,j}^{n+1} = {} & \frac{23}{12}\left(\left[-J(\psi, \omega)\right]_{i,j}^{n} \cdot \Delta t - \frac{g}{\theta_0}\frac{\theta_{i+1,j}^{n} - \theta_{i-1,j}^{n}}{2\Delta x} \cdot \Delta t\right) \\ & - \frac{16}{12}\left(\left[-J(\psi, \omega)\right]_{i,j}^{n-1} \cdot \Delta t - \frac{g}{\theta_0}\frac{\theta_{i+1,j}^{n-1} - \theta_{i-1,j}^{n-1}}{2\Delta x} \cdot \Delta t\right) \\ & + \frac{5}{12}\left(\left[-J(\psi, \omega)\right]_{i,j}^{n-2} \cdot \Delta t - \frac{g}{\theta_0}\frac{\theta_{i+1,j}^{n-2} - \theta_{i-1,j}^{n-2}}{2\Delta x} \cdot \Delta t\right) + \omega_{i,j}^{n} \end{aligned} \tag{6}$$

$$\theta_{i,j}^{n+1} = \frac{23}{12}\left[-J(\psi, \theta)\right]_{i,j}^{n} \cdot \Delta t - \frac{16}{12}\left[-J(\psi, \theta)\right]_{i,j}^{n-1} \cdot \Delta t + \frac{5}{12}\left[-J(\psi, \theta)\right]_{i,j}^{n-2} \cdot \Delta t + \theta_{i,j}^{n} \tag{7}$$

Finally, numerical diffusion was added using a FTCS scheme for both vertical velocity and potential temperature. The temperature diffusivity was equated to the artificial viscosity for vertical velocity to ensure that Prandtl number = 1.

$$\theta_{i,j}^{n+1} = \theta_{i,j}^{n-1} + K_\theta \frac{2\Delta t}{(\Delta x)^2}\left(\theta_{i+1,j}^{n-1} - 2\theta_{i,j}^{n-1} + \theta_{i-1,j}^{n-1}\right) + K_\theta \frac{2\Delta t}{(\Delta z)^2}\left(\theta_{i,j+1}^{n-1} - 2\theta_{i,j}^{n-1} + \theta_{i,j-1}^{n-1}\right) \tag{8}$$

$$\omega_{i,j}^{n+1} = \omega_{i,j}^{n-1} + \nu \frac{2\Delta t}{(\Delta x)^2}\left(\omega_{i+1,j}^{n-1} - 2\omega_{i,j}^{n-1} + \omega_{i-1,j}^{n-1}\right) + \nu \frac{2\Delta t}{(\Delta z)^2}\left(\omega_{i,j+1}^{n-1} - 2\omega_{i,j}^{n-1} + \omega_{i,j-1}^{n-1}\right) \tag{9}$$

A time step of 0.5 seconds was used to ensure that Courant number (C) remained below 1 and that Von Neumann number (s) remained below ¼ for all three resolutions: 101 x 101 (low), 202 x 202 (base), 404 x 404 (high). As Courant number changes during the simulation, Figure 1 is a plot of C(max) for each time step for each of the three resolutions. Here, C(max) is defined in the same was as in Modeling Task 6 and s(max) is defined in the same way as in Modeling Task 4.

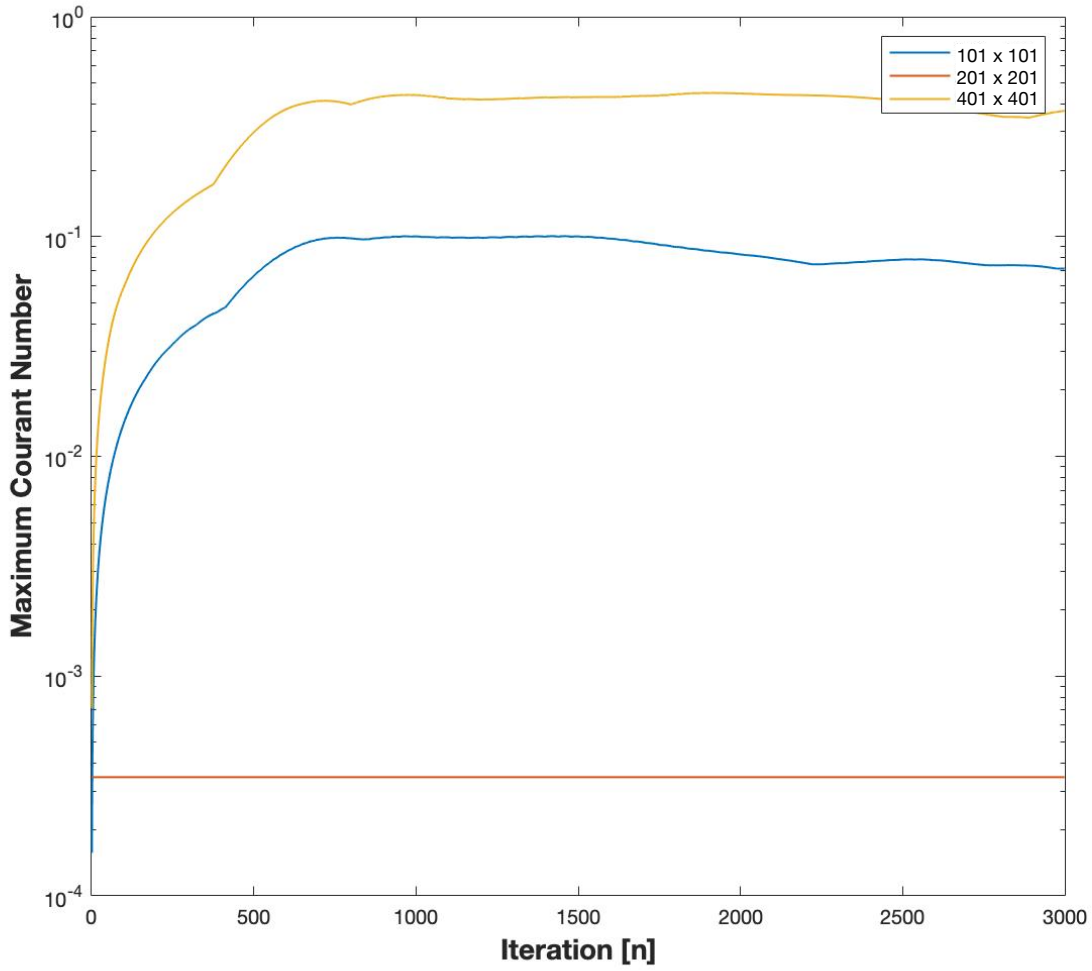

As is shown in **Figure 1**, the choice of $\Delta t = 0.5$ seconds ensures that C(max) stays below 1 for all three resolutions for the duration of the simulation. This ensures that the numerical viscosity is positive and that there is no amplification error in the solution.

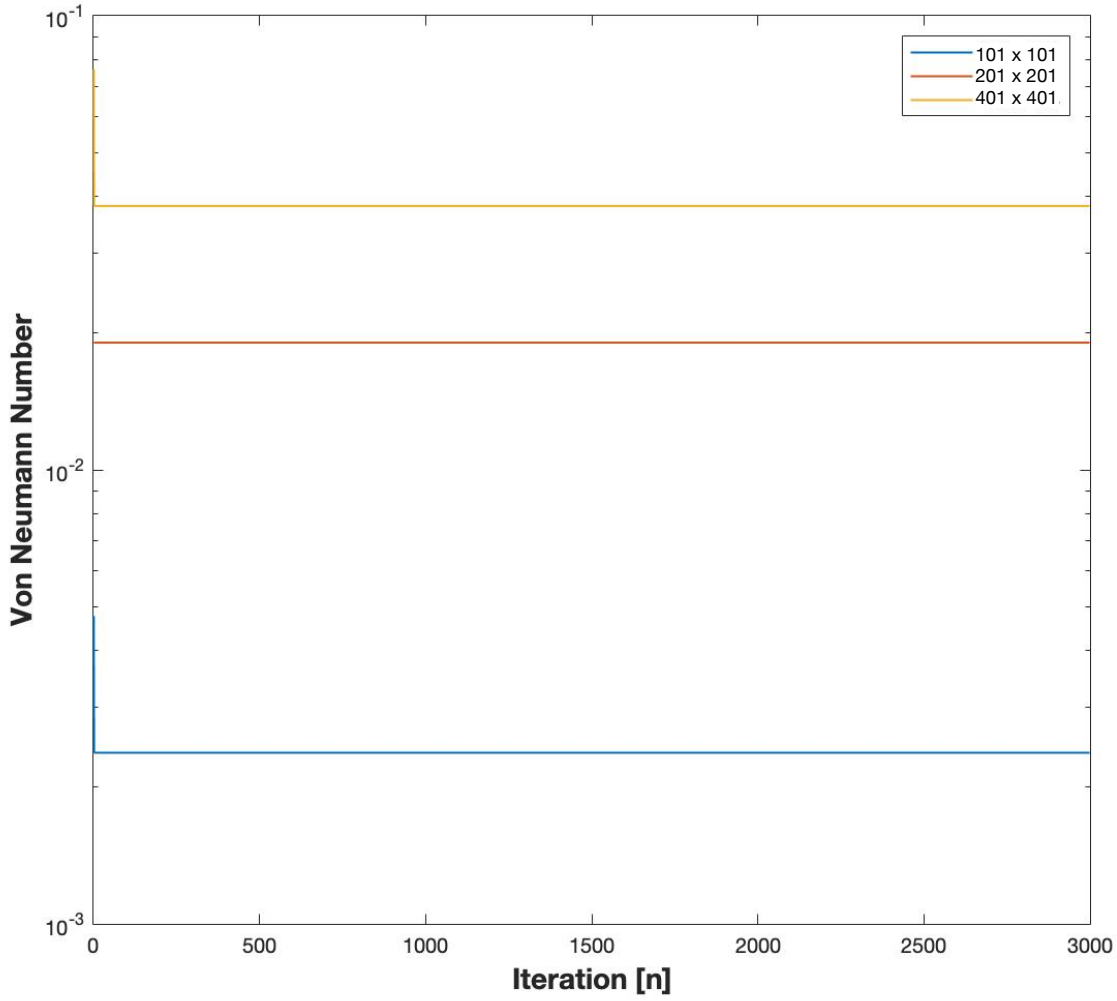

Von Neumann number is determined by diffusivity, which remained unchanged in the simulation and was the same in both the x and the z directions. We see in **Figure 2** that the difference between the solutions arises from the differences in Δx. Δx = 20m in the low resolution case, Δx = 10m in the base case, and Δx = 5m in the high resolution case.

Diffusivity for both potential temperature and vertical velocity was determined by first calculating U, the velocity scale.

With $U = \sqrt{\frac{2gr_0 \Delta\theta}{\theta_0}}$ and Reynold's number = 1500, we have diffusivity = $2r_0U / 1500 = 0.952902$.

This was value was used for all simulations.

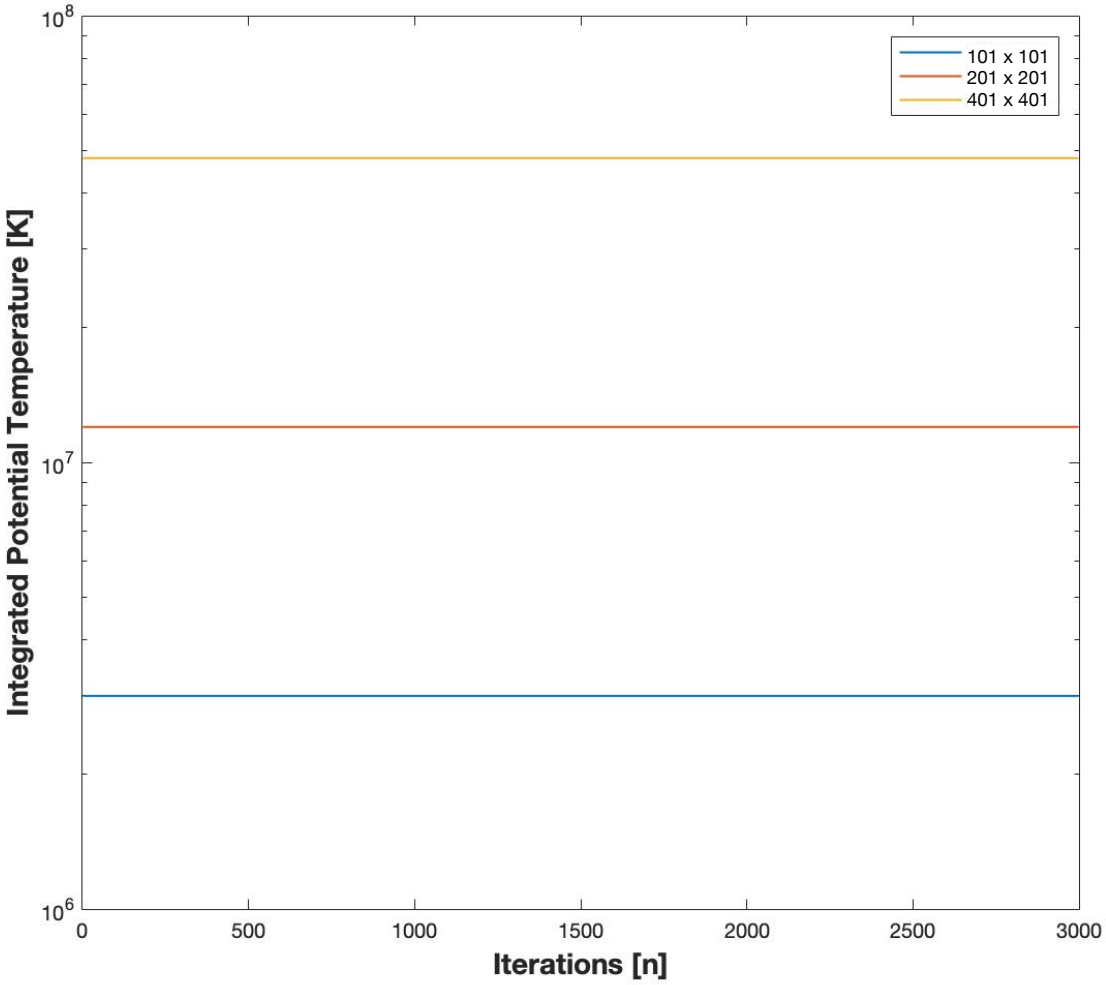

A note on stability can be made by looking at how integrated potential temperature is conserved throughout the simulation. As can be seen in **Figure 3**, all three resolutions are able to conserve the total potential temperature within the domain for the entire 1500 seconds of observation.

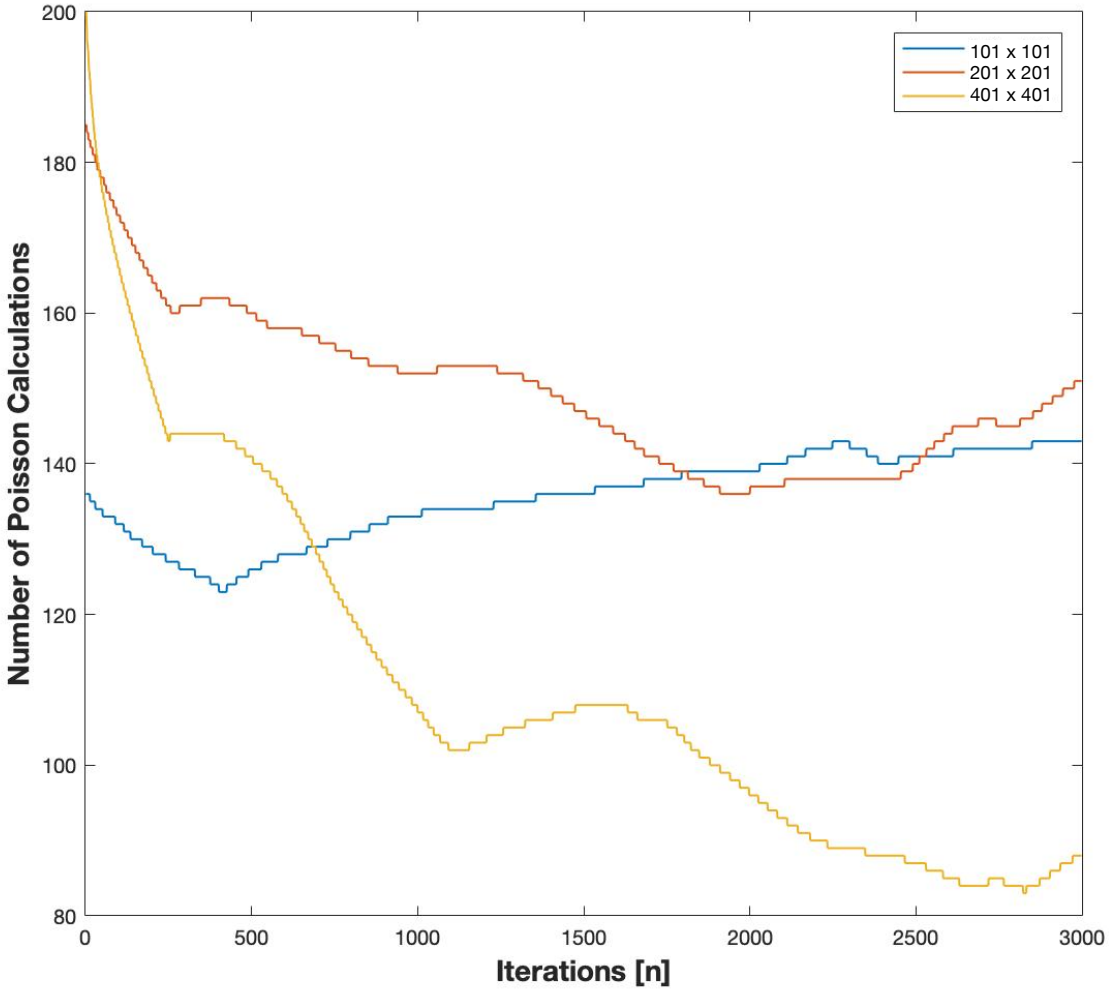

Figure 4 shows the number of Poisson calculations made to determine the stream function at each time step. The stream function was set to 0 after calculating vertical velocity and potential temperature to force the solution to enter the loop with the Poisson solver. In the case of the base and high resolutions, we see that the number of calculations generally decreases. The low resolution case shows an increase in the number of calculations, presumably due to greater degrees of changes as a result of the low resolution.

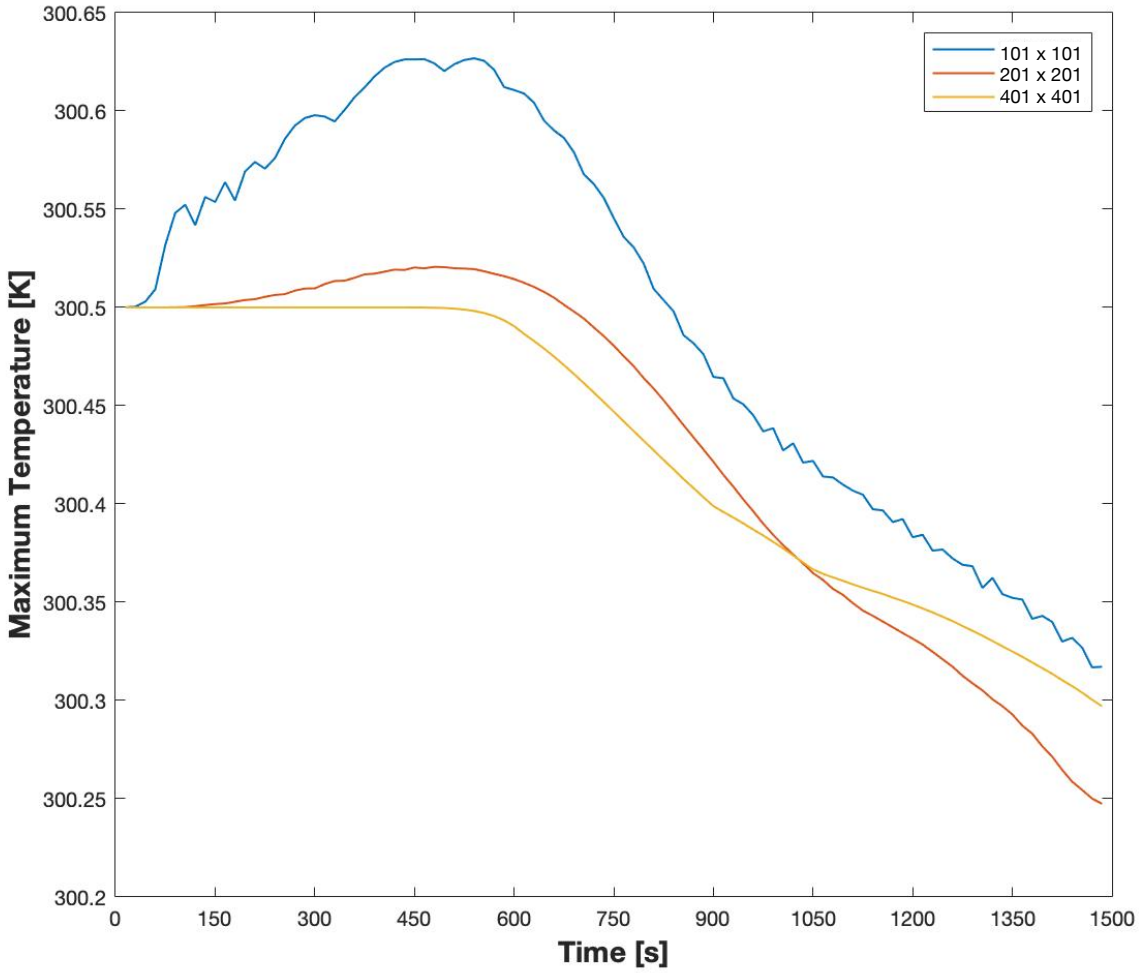

Finally, **Figure 5** records the maximum temperature within the domain at each time evolution. The low resolution notes first an increase in maximum temperature from 300.5K to almost 300.65K before the decrease in temperature begins as a result of the rising and diffusing of the thermal bubble. The base case resolution also notes a slight increase in maximum temperature of less than 0.25K before the same decrease is observed. The high resolution case shows that the thermal bubble retains its maximum temperature while it rises for the first 600 seconds, after which diffusion causes this maximum to decrease.It is also interesting to note that the rate of decrease in all three simulations is similar from 600 to 900 seconds. After this, the slope decreases for all three resolutions but to different extents or degrees.

The following time steps were plotted to compare the solutions for each of these resolutions: 900, 1350, 2100, and 2970 seconds. These times delineate first the similarities between the solutions and the evolution of the differences which result in the above explained trends in maximum temperature.

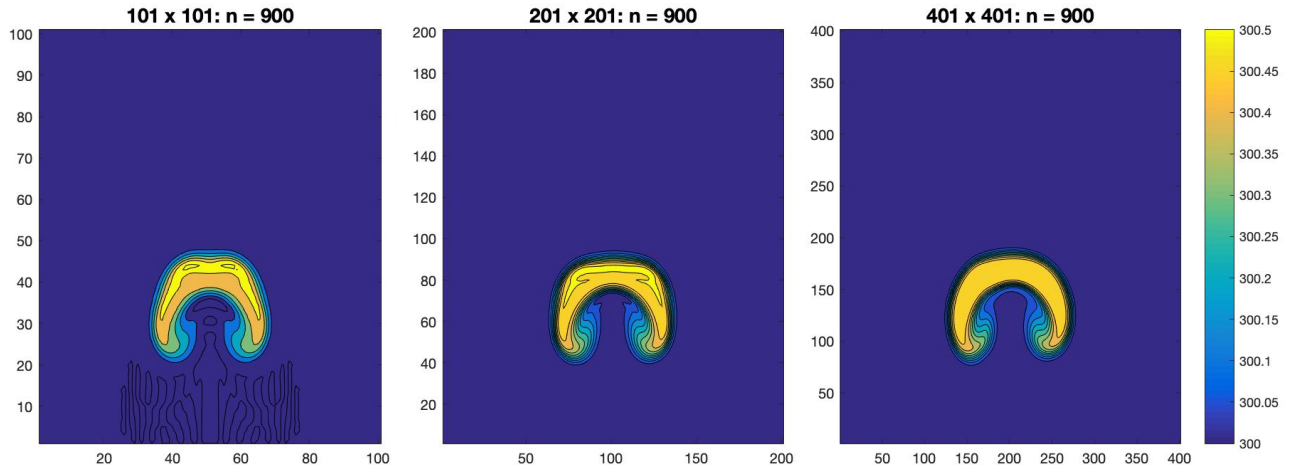

From left to right, **Figure 6** shows the rising motion of the thermal plume at different resolutions. Symmetry is retained in all three resolutions up until this point (450 seconds).

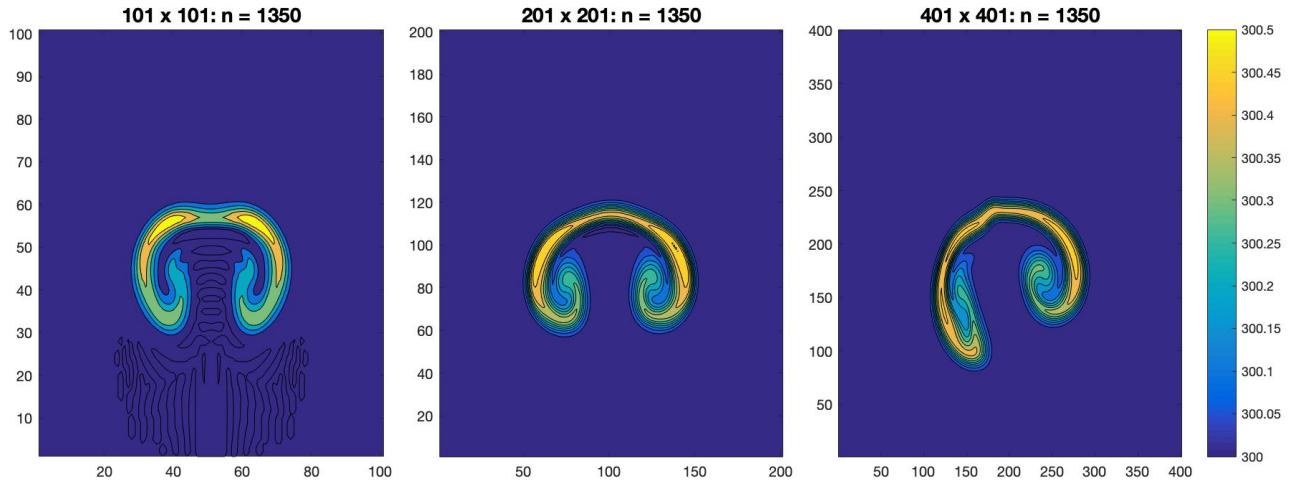

Figure 7 shows that the highest resolution solution loses symmetry first. It seems that the left lobe of the rising plume begins to rotate about itself and fails to advect at the same speed as the right side. This could possibly be due to the SOR method of solving the Poisson equation which goes from left to right, bottom to top, resulting in asymmetric evolutions of each part of the thermal plume as a result of using a mix of past and current stream function values in the domain. At this point (675 seconds) it is important to note that the base resolution looks similar to the the snapshot in the research paper (these similarities will be analyzed later). The lower resolution does not seem to have a secondary thermal plume evolving from the point at the top. This is observed in the base and high resolution plots as well as in the research paper.

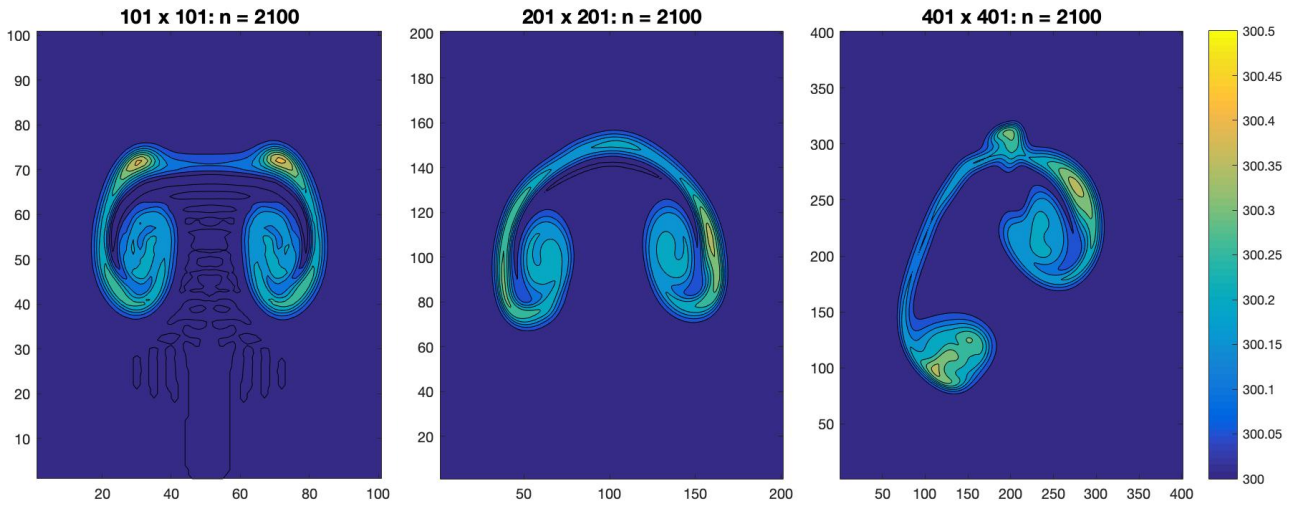

Figure 8 shows the increasing asymmetry in the base resolution. Unlike the high resolution plume, the base case does not have an asymmetrical advection. The difference is slightly more subtle and suggests that the right lobe of the thermal plume carries more heat than the left. The low resolution shows that the thermal plume is now beginning to split into two swirls. Here, symmetry is preserved to a greater degree even after 1050 seconds.

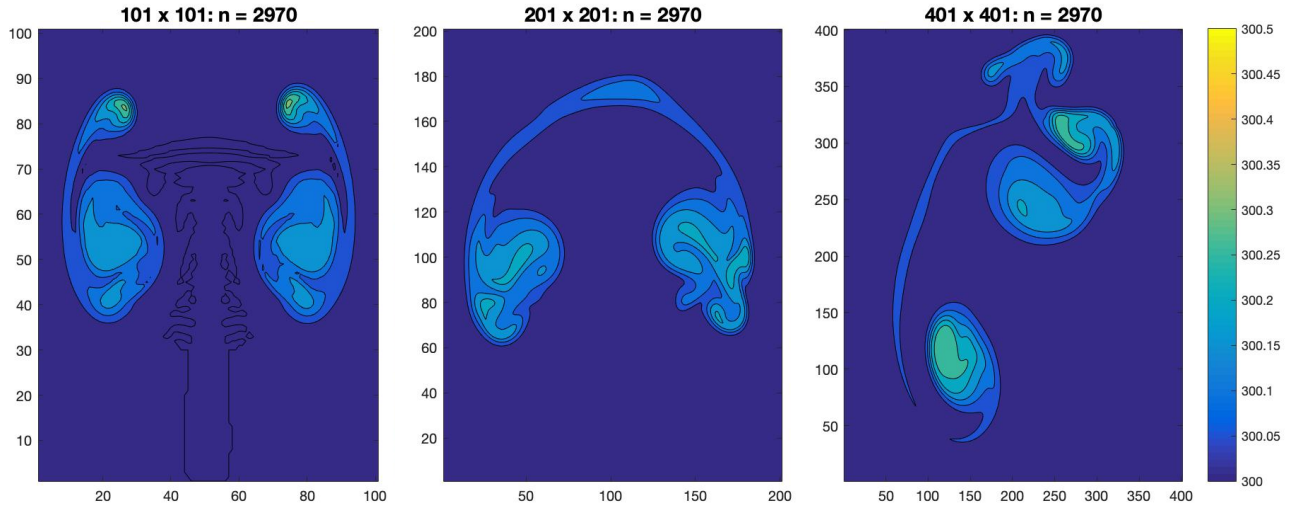

Figure 9 shows the solutions at the end of the run. By 1485 seconds, the low resolution shows that the plume does in fact split into two different lobes. The base resolution still has them connected but the two lobes are very clearly asymmetrical in both shape and height (z-coordinate) now. The high resolution case has a very clear secondary thermal plume evolving at the top while the two main lobes are very differently evolving.

To compare these simulations with the plots in the research paper, we will first determine the time steps to look at. For the low, base, and high resolutions discussed above, full solutions were saved every 30 time steps or every 15 seconds. This means we will only be comparing plots which are closest in time but may not correspond to the same second of time evolution.

The research paper presents us with plots made at $\tau = 2$, 5, and 7. This approximately corresponds to the times: 174.90, 436.26, and 612.17 seconds.

The closest plots made using the above resolutions are at times 180, 435, and 615 seconds (or 360, 870, and 1230 iterations).

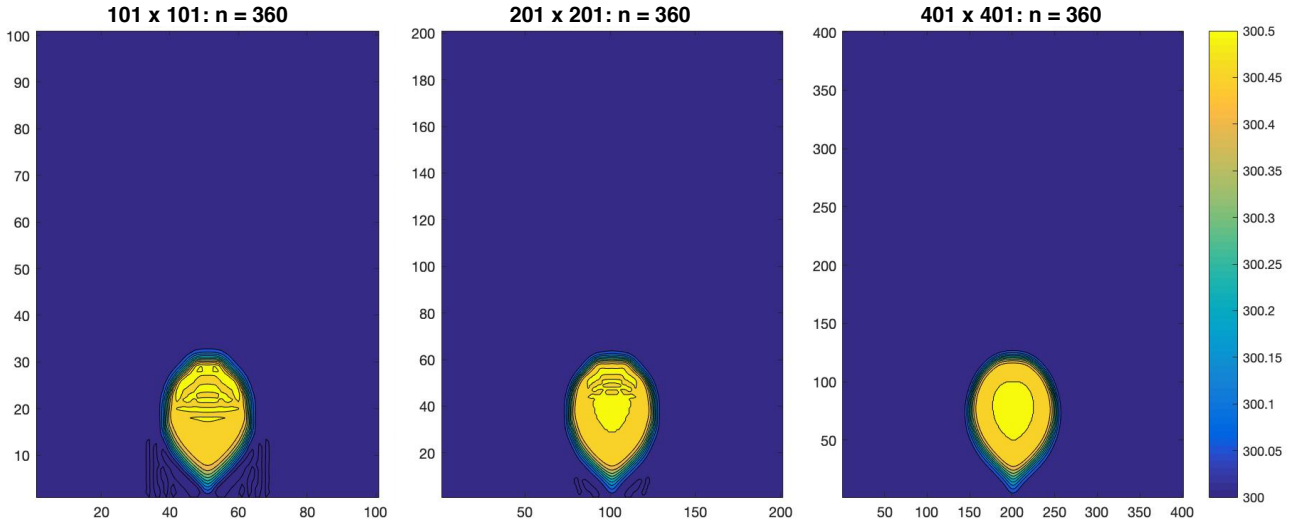

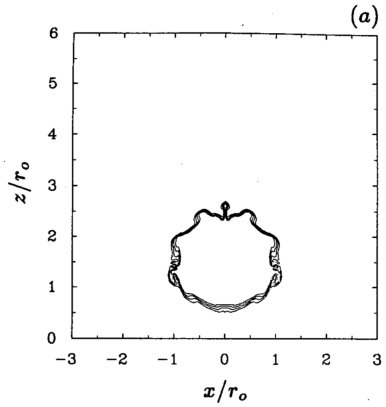

Figure 10 can be compared to Figure 3(a) in the paper. The greatest difference between these three solutions and the one in the paper is the lack of rippling on the edges of the plume. There is also a small point beginning to evolve at the top of the figure on the left while the figures above do not show this. The high resolution shows the most perfect solution. There are clear concentric oval-shaped contour lines showing a high temperature bubble surrounded by lower temperature. The base case and low resolution are showing ripples at the top of this rising bubble. In fact, the low resolution seems to also have a distinct computational mode which follows behind the bubble and advects out along the wall where z = 0.

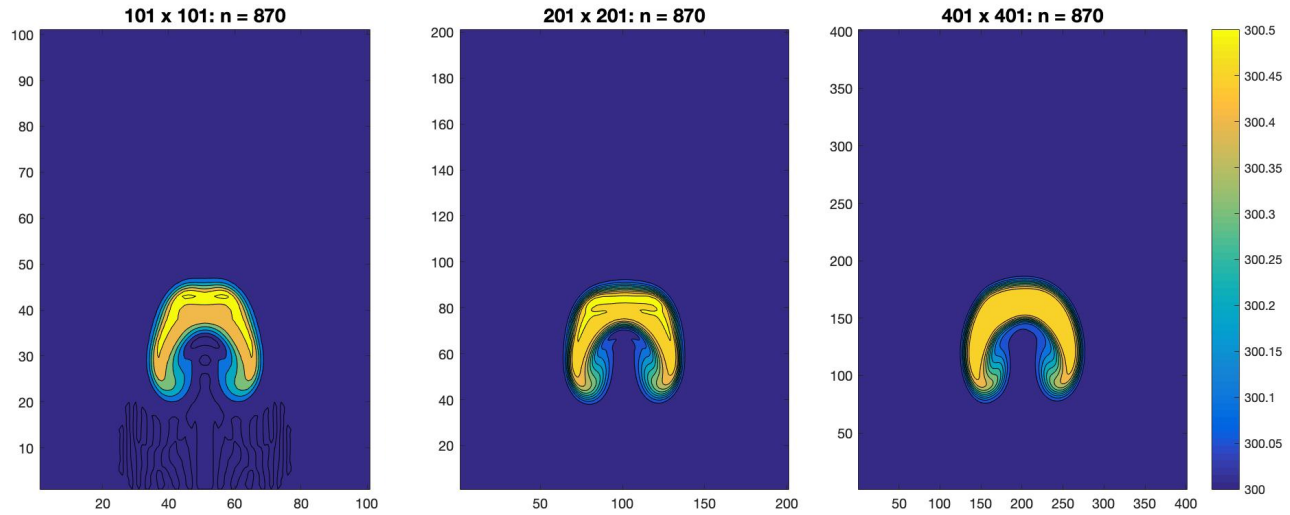

Figure 11 shows the computational mode in the low resolution more clearly. The top of the plume in the low resolution also looks more like the figure on the right due to the flat top. However, all three figures above lack the detail in the evolving ripples and the secondary evolution on the top. It seems that the overall horse-shoe shape of the solution is consistent.

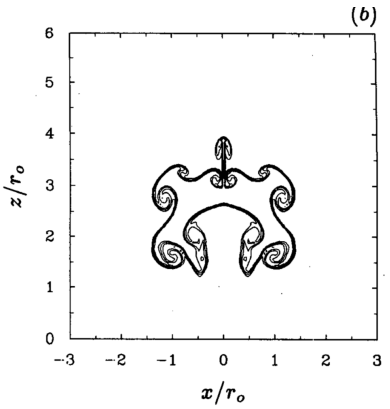

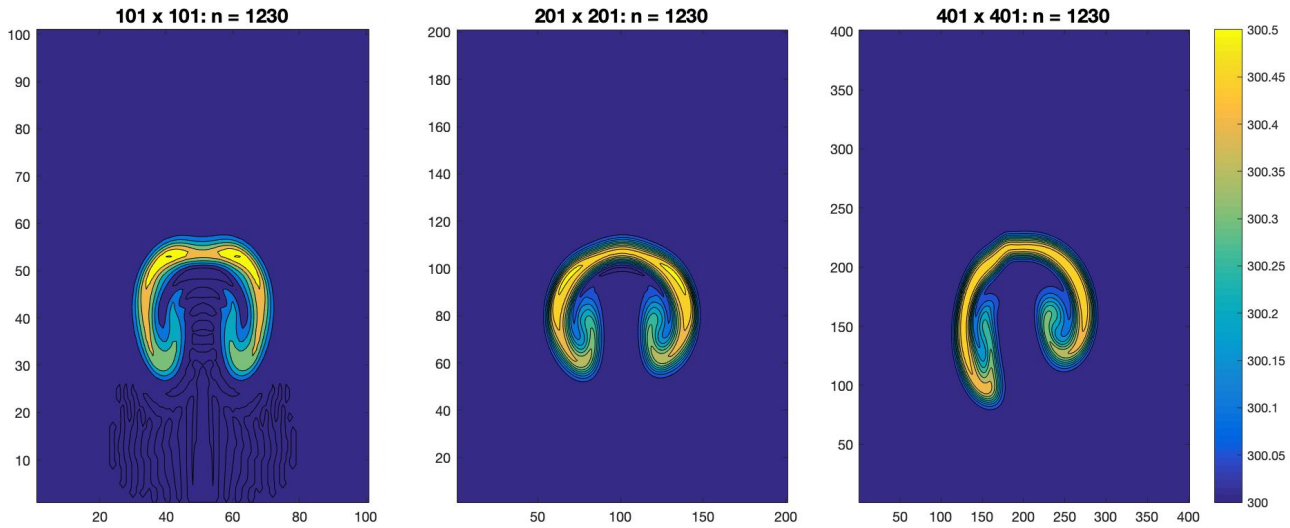

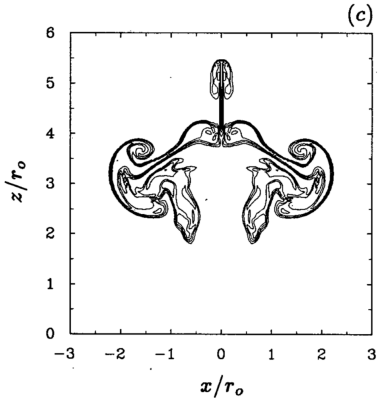

Figure 12 shows us that at this point in the simulation, the high resolution solution is beginning to lose its symmetry while the base case has retained its horse-shoe shape. The plot in the paper is shown on the left. We can see that the plume is becoming more clearly elongated in the x-direction with parts of it curling up while the above simulations show the lagging parts of the plume curling in/down.

From these conclusions, we can say that the solution used here is equipped to handle or capture the general evolution of a rising thermal plume in terms of allocating bands or regions of differing temperatures. In general, this simulation works best when there is a large enough temperature gradient that can be captured in the spatial grid. When there is a smaller resolution, the computational mode that tails the solution is more prominent. I think that the best solution overall was captured by the base case. This may have something to do with the maximum Courant number remaining the most stable and the lowest for this resolution (as seen in **Figure 1**).